



A mitochondria-targeted thiazoleorange-based photothermal agent for enhanced photothermal therapy for tumors

Wangqing Bian^a, Zhenxing Pan^a, Yakun Wang^a, Wei Long^a, Zefeng Chen^a, Niping Chen^a, Yaoxun Zeng^a, Jiongpeng Yuan^a, Xujie Liu^a, Yu-Jing Lu^a, Yan He^{a,*}, Kun Zhang^{a,b,*}

^a Allan H. Conney Laboratory for Anticancer Research, School of Biomedical and Pharmaceutical Sciences, Guangdong University of Technology, Guangzhou 510006, China

^b School of Biotechnology and Health Sciences, Wuyi University, Jiangmen 529020, China

ARTICLE INFO

Keywords:

Organic small molecules
Phototheranostic agents
Photothermal therapy
Mitochondria-targeted
Thiazole orange
Hyperpyrexia

ABSTRACT

Organic small molecules with near-infrared (NIR) absorption hold great promise as the phototheranostic agents for clinical translation by virtue of their inherent merits such as well-defined chemical structure, high purity and good reproducibility. Probes that happen to be based on cyanine dyes exhibit strong NIR-absorbing and efficient photothermal conversion, representing a new class of photothermal agents (PAs) for photothermal therapy (PTT), and taking into account the heat susceptibility of Mitochondria (Mito), we designed and prepared a mitochondria-targeted organic small molecule (Mito-BWQ) based on thiazole orange maternal unit that can effectively kill tumor cells through the hyperpyrexia generated in the lesions under exogenous laser irradiation. The Confocal laser scanning microscope was employed to determine the preferential targeting of Mito-BWQ to the mitochondria of MCF-7 cells and U87 cells. When subjected to 600 nm laser radiation, Mito-BWQ produced an increase in temperature in test systems and this increase was dependent on both the laser power and probe concentration. In vitro tests, cytotoxicity was observed when cells were incubated with Mito-BWQ and exposed to laser irradiation. The PTT in vivo also showed that Mito-BWQ performed remarkably in tumor inhibition. This study thus provides a vital starting point for the creation of thiazole orange-based PTT formulations and promotes further advances in the field of PAs-based anticancer research and therapy.

1. Introduction

Despite great progress in cancer therapy, malignant tumors such as breast cancer[1], which has a high incidence of female origin in the breast, and glioma[2], which has a high morbidity of intracranial origin in the neuroepithelium, remain a threat to people's health and will become the number one killer of modern society[3]. Traditional cancer therapies, including surgery, chemotherapy, and radiotherapy, have been in a bottleneck due to their severe side effects and inefficiency in achieving good prognosis[4,5]. Opportunistically, PTT adopts NIR radiation with strong penetrating power to tumor tissues and increases the temperature of lesions by photothermal conversion to destroy cancer cells[6,7]. Moreover, the tumor is more sensitive to hyperpyrexia of 42–45 °C than normal tissues on account of the vascular inhomogeneity of the tumor site[8,9]. The most noteworthy feature of PTT is that it is non-invasive or minimally invasive, so that patients will not feel very

painful during the treatment, and the heat generated only affects the surrounding cells, without triggering a systemic reaction, and the side effects will be significantly reduced[6,7].

To improve the depth, range and efficiency of PTT, it is indispensable to construct PAs that absorbs NIR light and generates heat. And the ideal PAs should have low toxicity, high absorption and high photothermal conversion efficiency (PCE) in the NIR window (650–950 nm). With the development of nanotechnology, a great deal of nanomaterials with strong absorption in the NIR region demonstrate certain prospects for PTT applications. Among them, inorganic nanomaterials including gold nanomaterials with different structures[10,11], carbon nanomaterials[12], palladium nanosheets[13], copper sulfide nanomaterials[14] and other novel nanomaterials[15,16] have been used as PAs in PTT. However, inorganic PAs such as these are not readily degradable in vivo and have potential long-term toxicity issues that immensely limit their applications. For example, despite the outstanding photothermal conversion capacity of

* Corresponding authors at: Allan H. Conney Laboratory for Anticancer Research, School of Biomedical and Pharmaceutical Sciences, Guangdong University of Technology, 100 Wai Huan West Road, Guangzhou Higher Education Mega Center, Guangzhou 510006, China.

E-mail addresses: heyuan129@gdut.edu.cn (Y. He), kzhang@gdut.edu.cn (K. Zhang).

<https://doi.org/10.1016/j.bioorg.2021.104954>

Received 3 March 2021; Received in revised form 14 April 2021; Accepted 28 April 2021

Available online 30 April 2021

0045-2068/© 2021 Elsevier Inc. All rights reserved.

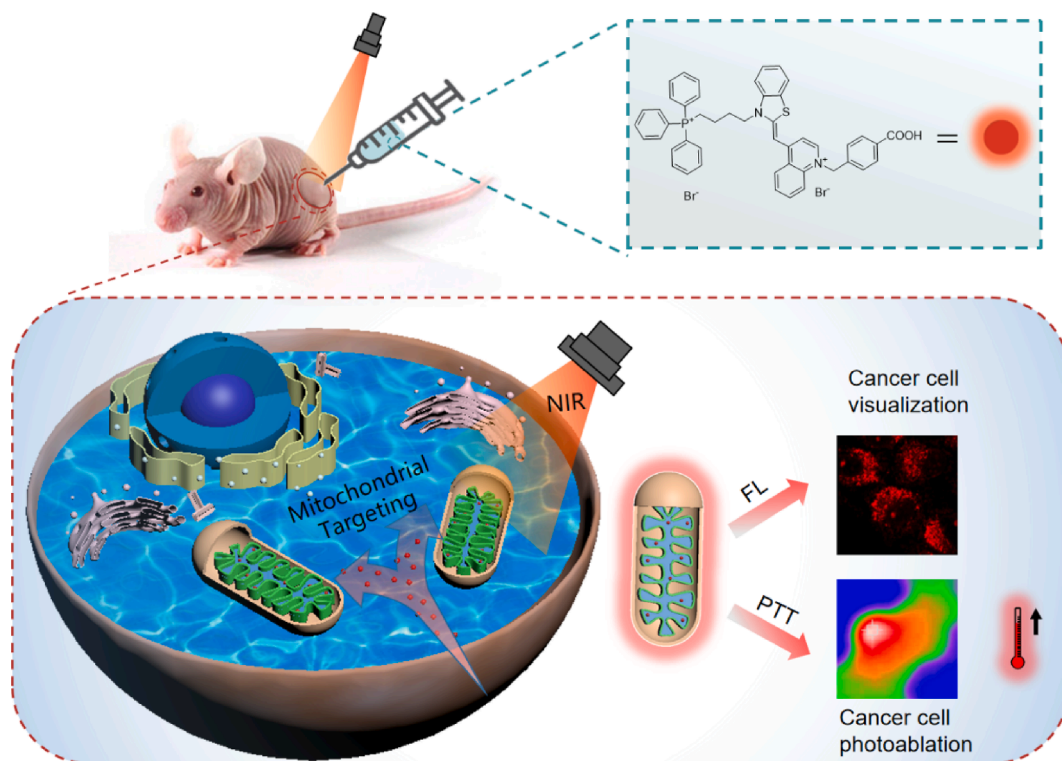


Fig. 1. Schematic illustration of fluorescence imaging and enhanced photothermal therapy by mitochondria-targeting thiazole orange (Mito-BWQ).

carbon nanotubes, the compounds based on them tend to accumulate in the liver and kidneys, causing varying degrees of damage to them. Some studies have injected carbon nanotubes into the abdominal cavity of mice and found them to be carcinogenic similar to asbestos[17–20].

In recent years, PAs based on organic materials including organic NIR dyes[21], porphyrin liposomes[22], and polymers have been favored by researchers because they are significantly better than inorganic materials in terms of biosafety. Among them, organic small molecule photothermal agents (OSPAs) are gradually being developed as PAs for PTT owing to their intrinsic prominent biodegradability, low toxicity and synthetic flexibility[21,23]. In addition, mitochondria are indispensable organelles responsible for most of the energy supply of producing cells, play a key role in the processes of apoptosis and cell death, and are particularly sensitive to changes in cardiolipin metabolism or heat shock, which can be easily damaged by hyperthermia[24–26]. Therefore, mitochondrial heat transfer mediated by various forms of nanostructures[27–29] has been attempted adopting mitochondrial guides, including triphenylphosphonium (TPP) cations[30], mitochondrial phospholipid cardiolipids[31], mitochondrial penetrating peptides[32], oligomeric carbohydrate scaffolds, mitochondrial targeting sequences[33], and vesicle-based transporter systems.

Recently, Jung et al[34] reported a mitochondria-targeted hyperthermic inducer that employs TPP-bound nanoparticles to trigger mitochondrial dysfunction, leading to apoptosis. OSPAs provide benefits over other nanomaterials, including improved safety in many cases and ease of preparation and modification. Thus, we believe that great advantages exist for mitochondria-targeted PAs based on organic small molecules. However, there are two tough issues that need to be addressed in advance: 1) the design and synthesis of original OSPAs with high NIR absorption, low toxicity, and high PCE to offer an alternative to PTT; and 2) the efficient introduction of mitochondria-targeted ligands into OSPAs to enhance their therapeutic efficacy.

Cyanate dyes, with remarkable photophysical properties and low biotoxicity, are a range of extraordinary OSPAs that have been used as imaging and therapeutic agents to attain therapeutic integration[35]. For example, indocyanin green (ICG), approved by the FDA as a medical imaging agent, has also been served as a PA. Herein, in this study, we set out to construct a new family of cyanate dyes based on thiazole orange OSPAs (Fig. 1), referred to as Mito-BWQ, with a large π -conjugated system that absorbs NIR and efficiently converts light to heat. Furthermore, the alkyl bromide group can be readily functionalized by triphenylphosphonium to enable targeting

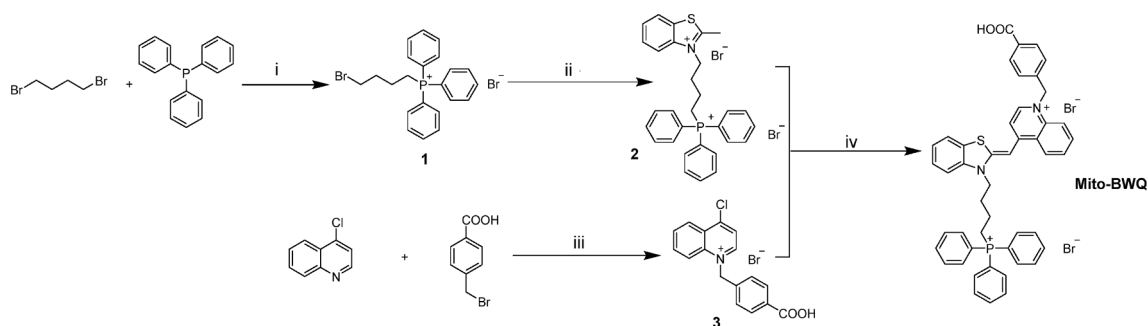


Fig. 2. Synthesis of Mito-BWQ. (i) Toluene, 120°C, 12 h; (ii) 2-Methylbenzothiazole, CH₃CN, 120°C, 36 h; (iii) 1,2-dichlorobenzene, CH₃CN, 110°C, 24 h; (iv) MeOH, TEA, P-methylbenzene sulfonic acid, 30°C, 4 h.

of mitochondria and induce cell necrosis with hyperpyrexia. In a series of *in vitro* and *in vivo* tests, Mito-BWQ showed high PCE, light-induced cytotoxicity, good biocompatibility, and admirable fluorescence imaging capability and tumor growth suppression, which will be a good choice for PTT. And to the best of our knowledge, this work is the first to report OSPAs based on the thiazole orange maternal unit with mitochondria as the primary site of action for enhanced PTT of tumors.

2. Materials and methods

2.1. Materials

In this study, all chemicals and reagents were purchased from commercial in AR grade and were used without further purifications. phosphate-buffered saline (PBS, pH = 7.4), Fetal bovine serum (FBS), DMEM medium, trypsin Cell Counting Kit (CCK-8), 4,6-diamidino-2-phenylindole (DAPI) were purchased from Gibco, USA. Calcein-AM and propidium iodide (PI) were purchased from YEASEN (Shanghai, China). All other reagents were purchased from Aladdin.

2.2. Synthesis of OSPA (photo-thermal thiazoleorange)

The putative mitochondria-targeted thiazoleorange (Mito-BWQ) and a nontargeted thiazoleorange (BWQ) control were synthesized as outlined in Fig. 2. Briefly, the synthesis entailed alkylation reaction of 1, 4-dibromobutane with triphenyl phosphine gives 1 and the reaction with 2-methylbenzothiazole gives 2. 3 was obtained by alkylation reaction of 4-chloro-dimethylquinoline with p-bromomethylbenzoic acid, and then 2 was added to methanol, and triethylamine (TEA) was added as catalyst for reaction, so that the π -conjugated system was expanded, and the target compound was obtained and gave ^1H NMR, ^{13}C NMR spectral and mass spectrum analytical data consistent with their proposed structures (Figure S2-S10).

2.3. Calculation of the fluorescence quantum yield

The fluorescence quantum yields of Mito-BWQ and BWQ were calculated the standard of fluorescein ($\Phi = 0.95$) in the condition of 1% NaOH ethanol, and Φ_x were measured according to the following equation [7]:

$$\Phi_x = \Phi_{ST} \left(\frac{\text{Grad}_x}{\text{Grad}_{ST}} \right) \left(\frac{\eta_x^2}{\eta_{ST}^2} \right) \quad (\text{A1})$$

Where, the subscript ST is the standard and the subscript x is the test sample. Φ represents the fluorescence quantum yield value. Grad is the slope of the curve with the integrated fluorescence intensity as the ordinate, the ultraviolet absorbance as the abscissa, and η is the refractive index of the solvent used.

2.4. Calculation of the photothermal conversion efficiency

The photothermal conversion efficiencies (η) were measured according to a previously described method [36]:

$$\eta = \frac{hs(T_{Max} - T_{Surr}) - Q_{Dis}}{I(1 - 10^{-A730})} \quad (\text{A2})$$

h is the heat transfer coefficient, s is the surface area of the container, and the value of hs is determined from the equation (A3). Q_{Dis} represents heat dissipated from the laser mediated by the solvent and container. I is the laser power and A is the absorbance at 600 nm.

$$hs = \frac{mC}{\tau_s} \quad (\text{A3})$$

m is the mass of the solution containing the photoactive material, C is the specific heat capacity of the solution, and τ_s is the associated time constant, which can be determined from equation (A4).

$$t = -\tau_s \ln(\theta) \quad (\text{A4})$$

θ is a dimensionless parameter, known as the driving force temperature, as calculated using equation (A5).

$$\theta = \frac{T - T_{Surr}}{T_{Max} - T_{Surr}} \quad (\text{A5})$$

T_{max} and T_{Surr} are the maximum steady state temperature and the environmental temperature, respectively.

2.5. Cell culture and confocal microscopy studies

MCF-7 cells and U87 cells were incubated in DMEM medium supplemented with 1% penicillin–streptomycin (v/v) and 10% (v/v) FBS at 37°C under a humidified atmosphere with 5% CO₂. The cells were treated and incubated with Mito-BWQ at 37°C under 5% CO₂ during the time mentioned in the text. For the confocal microscopic samples, the cells were passed and plated on glass bottomed dishes. The cells were washed three times with phosphate buffered saline and then imaged after further incubation in colorless serum-free media for 30 min. Fluorescence microscopy images of labeled cells were obtained with spectral confocal microscopes (*LSM 800 With Airscan). Tracking dyes for co-localization experiments were bought from Invitrogen. Other information is available in the figure captions.

2.6. In vitro PTT.

The cell viability assays was performed by a standard CCK-8 assay. MCF-7 cells and U87 cells (10⁴ cells/well) were seeded on 96-well plate and incubated for 24 h at 37 °C. The cells were treated with different concentrations of Mito-BWQ (0, 3, 6, 12, 25, 50 $\mu\text{g}/\text{mL}$) and incubated for 4 h at 37 °C. After incubation, the cells were washed three times and irradiated different times (0, 1, 2, 3, 4, and 5 min) with a 600 nm laser at 1.5 W/cm². On the one hand, MCF-7 cells (2.0 \times 10⁵ per dish) were seeded on 35 mm confocal dishes and allowed to stabilize for 24 h. The cells were then treated with different concentration Mito-BWQ (0, 3, 6, 12, 25, and 50 $\mu\text{g}/\text{mL}$) in 1 mL culture medium. After 4 h incubation, the cells were irradiated with a 600 nm laser (1.5 W/cm²) for 5 min to induce photothermal cytotoxicity. The mode of cell death was examined by using Calcein AM/PI staining kit, and the cells were imaged by OLYMPUS 20,112,167 inverted fluorescence microscope.

2.7. Animals and tumor Models.

Female Balb/c nude mice (18–20 g) were housed under aseptic conditions in small animal isolators with free access to food and water. All care and procedures of animals were approved by the University Ethics Committee for the use of experimental animals. To establish tumor xenograft models, MCF-7 cell suspensions (1 \times 10⁶ cells) were subcutaneously injected

into the flank of nude mice. A caliper was used to measure tumor sizes, and tumor volume (mm³) was calculated as (tumor major axis) \times (tumor minor axis)² /2.

2.8. In vivo FL

All the animal experiments were approved by the Guanzhong Medical Laboratory Animal Center. Balb/c nude mice (6–8 weeks) with subcutaneous-tumors in the lower right side of the back area were used as the animal models. The imaging experiments were carried out when the subcutaneous-tumors grew to 60 mm³ in diameter. The Mito-BWQ (1 mg/kg) was intratumorally injected into mice with normal saline as an aqueous solution (n = 5 in each group), and then FL images at different time points were acquired on an *in vivo* FL imaging system (FX PRO, Bruker).

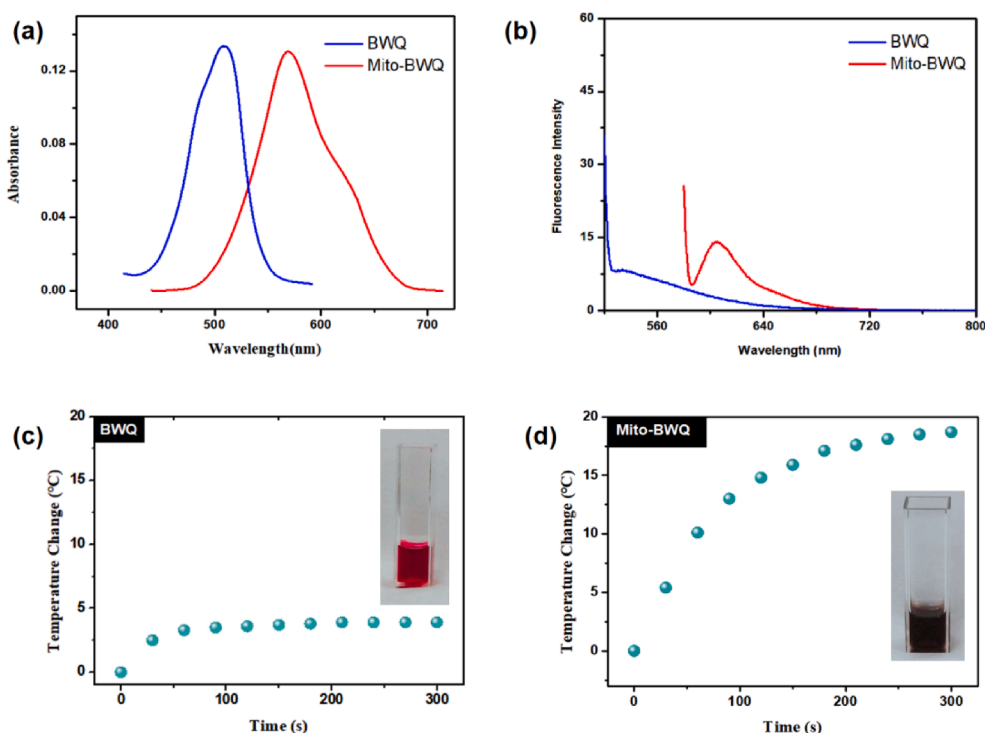


Fig. 3. Characterization and Photothermal heating curves of Mito-BWQ and BWQ. (a) UV absorption spectra and (b) Fluorescence emission spectra of BWQ and Mito-BWQ at the concentration of 1.5 μM in 10% DMSO-buffer solution (pH 7.4, 10 mM PBS). (c) BWQ and (d) Mito-BWQ (0.5 mM, respectively) dispersed in 50% DMSO – buffer solution (pH 7.4, 10 mM PBS) with 600 nm laser irradiation (1.5 W/cm^2) as a function of irradiation time.

2.9. In vivo thermal imaging

When the subcutaneous-tumors reached 60 mm^3 , Mito-BWQ (5 mg/kg) or PBS was intratumorally administered into the nude mice bearing MCF-7 tumors. Thermal imaging was presented by an HT-02 Handheld thermal imaging camera when the tumors were subjected to 600 nm laser with the power density of 1.5 W/cm^2 .

2.10. In vivo PTT and H&E Staining.

The tumor-bearing mice with average tumor volume around 100 mm^3 were divided into six groups treated with (1) PBS (laser-), (2) PBS (laser +), (3) laser, (4) Mito-BWQ (laser-), (5) Mito-BWQ (laser +). Mito-BWQ (5 mg/kg) was intratumorally injected into the nude mice with subcutaneous-tumors ($n = 5$ in each group). At 24 h after injection, the tumors were exposed to a NIR laser of 1.5 W/cm^2 for 5 min. The tumor photos at different time points before and after injection of Mito-BWQ were recorded to monitor the volume changes of tumors. The tumor inhibition ratio, the tumor sizes and mouse weight were measured at different time points. After the therapeutic period, mice were sacrificed. For hematoxylin and eosin (H&E) staining, briefly, slides of organs were fixed with 4% paraformaldehyde solution, after that dehydrated, performed H&E staining.

2.11. Statistical Analysis.

The results are expressed as the mean \pm standard error. Statistical comparisons between the two groups were performed using the two-tailed, unpaired Student's test. Statistical significance was indicated as * $P < 0.05$, ** $P < 0.01$, or *** $P < 0.001$.

3. Results and discussion

3.1. Characterization of thiazoleorange.

Initially, we explored the photophysical properties of Mito-BWQ and BWQ, the absorption and emission features of Mito-BWQ and BWQ were probed in dimethyl sulfoxide (DMSO) using UV – vis and fluorescence spectroscopy, respectively (Fig. 3). The absorption spectra exhibited an intense peak at 575 nm and 505 nm (Fig. 3a) with large molar extinction coefficients of 1.50 $\text{M}^{-1}\text{cm}^{-1}$ and 2.45 $\text{M}^{-1}\text{cm}^{-1}$ for Mito-BWQ and BWQ, respectively (Figure S13). The fluorescence maximum of Mito-BWQ and BWQ were observed at 606 nm and 535 nm (Fig. 3b), the fluorescence QYs (Φ_f) were calculated according to eq A(1) and found to be 0.029 and 0.022, respectively (Figure S13). In addition, preliminary investigation found that the buffer solution of Mito-BWQ resulted in a higher temperature rise than the corresponding buffer solution of BWQ under the same conditions (~ 19.2 $^\circ\text{C}$ vs ~ 3.6 $^\circ\text{C}$ for Mito-BWQ and for BWQ) (Fig. 3c – d). On the basis of these findings, we considered it likely that Mito-BWQ would prove effective as a PTT agent.

3.2. Photothermal conversion Efficiency.

To further explore the PCE of Mito-BWQ, the temperature of Mito-BWQ dispersed in phosphate buffered solution (PBS, pH 7.4) was determined as a function of the power density and concentration of NIR irradiation. We observed a significant increase in the temperature of the dispersed solution at 0.5 mM as the laser power density raised from 0 to 1.8 W/cm^2 (Fig. 4a-b). Furthermore, the temperature of the dispersed solution under irradiation with the 600 nm NIR laser at 1.5 W/cm^2 gradually boosted with enhancing Mito-BWQ concentration (Fig. 4c-d). The temperature of the solution increased by 25 $^\circ\text{C}$ within 2 min at 1 mM, whereas no such change was observed for the particle-free solution.

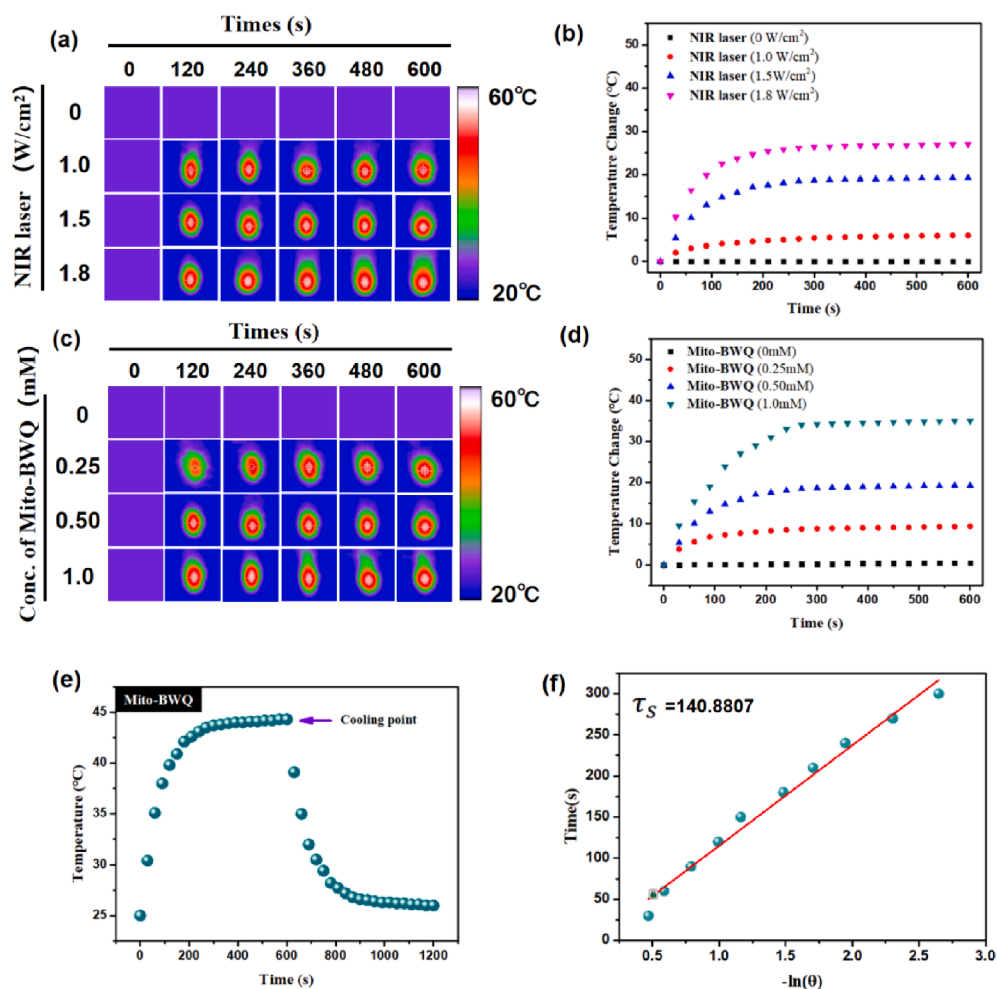


Fig. 4. Photothermal conversion utility of Mito-BWQ. IR thermal images of DMSO solutions of Mito-BWQ (a and c). Mito-BWQ concentration = 0.5 mM and irradiation intensities of 0, 1.0, 1.5, and 1.8 W/cm² at 600 nm (a) and 1.5 W/cm² irradiation (600 nm) at various Mito-BWQ concentrations (0, 0.25, 0.50, and 1.0 mM) (c) as a function of irradiation time. Photothermal heating curves for DMSO solutions of Mito-BWQ at constant 0.5 mM concentrations of Mito-BWQ and various laser irradiation intensities (0, 1.0, 1.5, and 1.8 W/cm², 600 nm) (b) and constant irradiation at 1.5 W/cm² with varying Mito-BWQ concentrations (0, 0.25, 0.50, and 1.0 mM, 600 nm) (d) as a function of irradiation time. Photothermal effects observed upon irradiating Mito-BWQ with 600 nm laser light (1.5 W/cm²) for 600 s and then stopping the irradiation (e). Time versus $-\ln(\theta)$ plot with θ being the driving force temperature, cf. eq S5) (f) obtained using the data recorded during the cooling period of the experiment outlined in (e). A Ti:Sa femtosecond-pulsed laser (Chameleon XR by Coherent, 200 fs pulse width, 90 MHz repetition rate) was used.

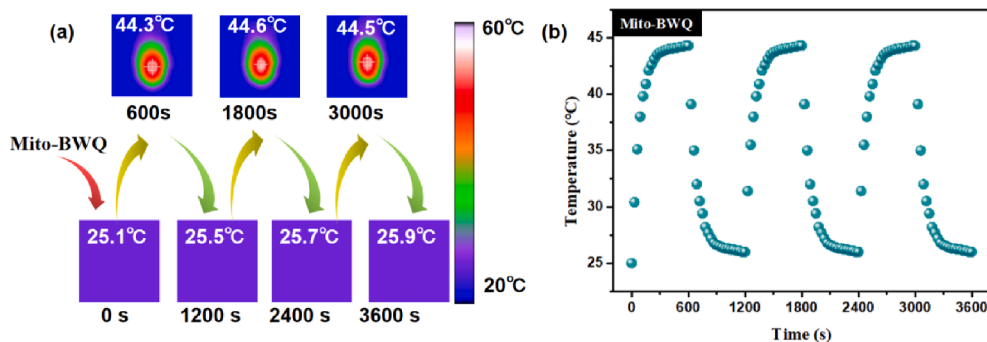


Fig. 5. Photostability of Mito-BWQ in DMSO. (a) IR thermal images of Mito-BWQ. (b) Curves showing the temperature change of Mito-BWQ over several ON/OFF cycles involving irradiation with a 600 nm laser (1.5 W/cm²) for 1 h followed by passive cooling.

These results reveal that the heat is generated by NIR irradiation of Mito-BWQ with good photothermal conversion. To more precisely evaluate the heat transfer utility of Mito-BWQs, their PCE was measured using the reported method [36]. As defined by equation (S8-S11), the efficiencies (η) of Mito-BWQ and BWQ were found to be approximately 35.6% and 10.1%, respectively. Moreover, due to the introduction of triphenylphosphine, the PCE of Mito-BWQ is more than doubled, which is much higher than that of reported mitochondria-targeted photothermal agents, such as IR825 ($\approx 17.4\%$) [37]. These results indicate that Mito-BWQ is an excellent OSPA candidate for PTT.

3.3. Photostability of Mito-BWQ.

Before applying the Mito-BWQ to cell studies, we measured its photostability. For this purpose, Mito-BWQ was passively cooled to room temperature after laser irradiation, and the cycle was repeated for 1 h. As shown in Fig. 5a-b, the maximum temperature increase in each cycle was $< 2.0\%$, so we concluded that Mito-BWQ is stable under 600 nm laser irradiation.

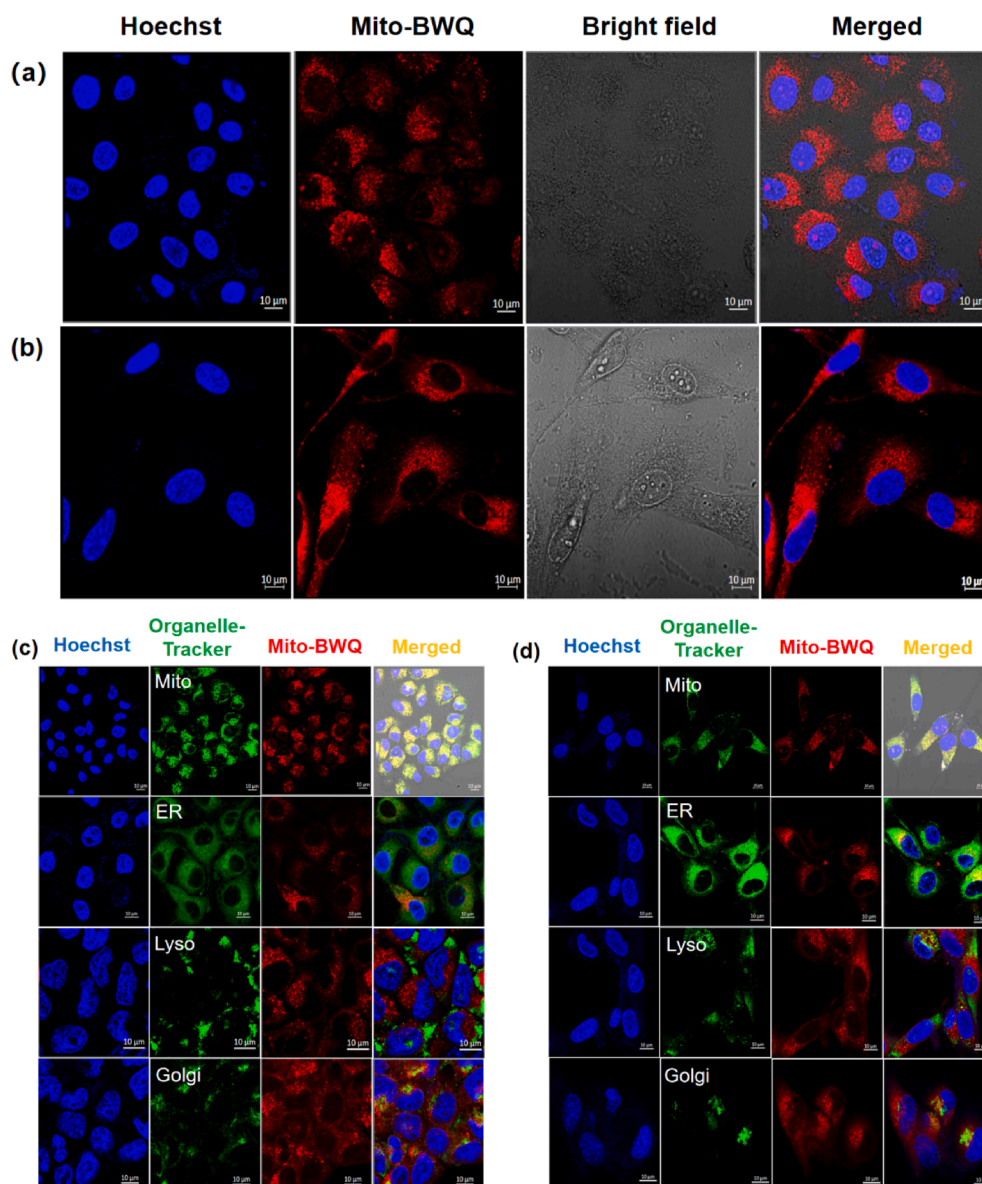


Fig. 6. Confocal fluorescence microscopic images of MCF-7 cells (a) and U87 cells (b) after incubation with Mito-BWQ for 30 min. Confocal images of Mito-BWQ-treated MCF-7 cells (c) and U87 cells (d) before imaging, the cells were stained with Mito-Tracker, ER-Tracker, Lyso-Tracker, and Golgi-Tracker. The cell nuclei were stained with Hoechst 33,342 (abbreviated as Hoechst).

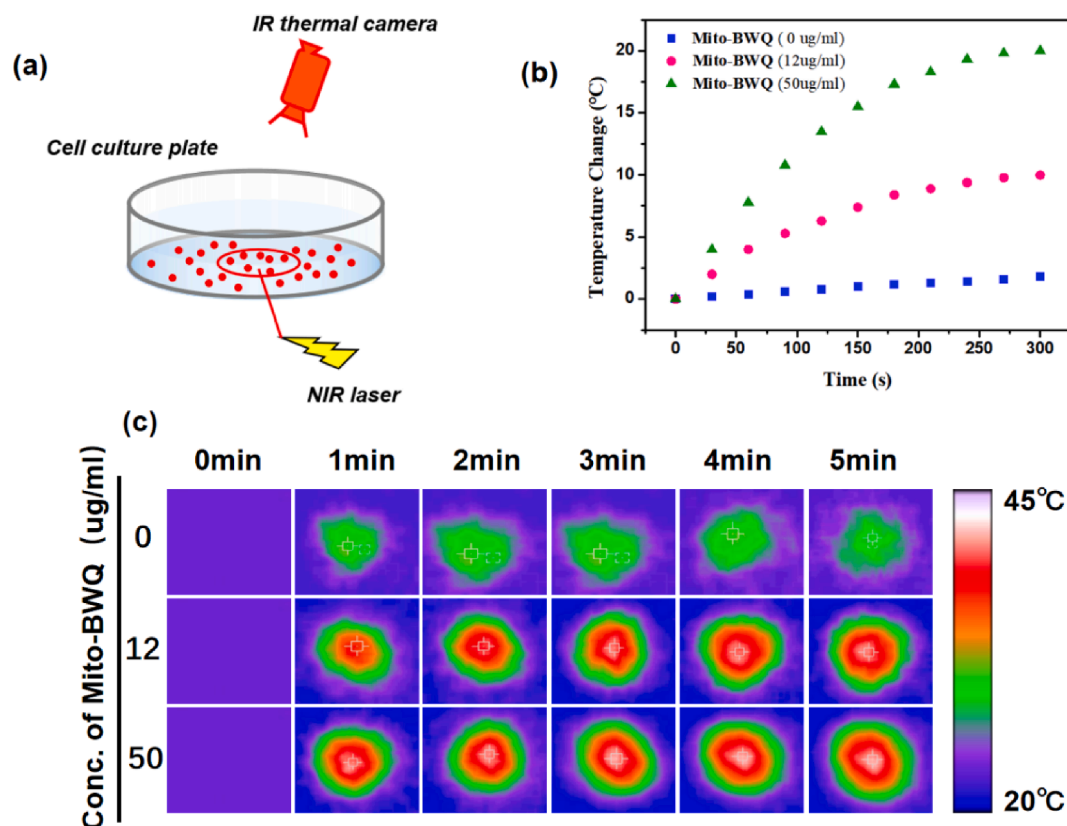


Fig. 7. Photothermal conversion efficiency of Mito-BWQ inside cells. (a) Schematic diagram of MCF-7 cells in a delta T dish loaded with Mito-BWQ upon NIR laser irradiation. The red circle shows the area of laser illumination. The local temperature change was monitored using an IR thermal camera. (b) Hyperthermia heating curves. (c) IR thermal images of MCF-7 cell media with Mito-BWQ at various concentrations (0, 12, and 50 µg/ml) as a function of irradiation time. (For interpretation of the references to colour in this figure legend, the reader is referred to the web version of this article.)

3.4. Confocal microscopy studies of Mito-BWQ.

To investigate the uptake of Mito-BWQ by cells, MCF-7 cells (Fig. 6a) and U87 cells (Fig. 6b) were incubated with Mito-BWQ for 30 min at 37 °C. The good uptake of Mito-BWQ by cells was confirmed by laser confocal microscopy. Prior to studying the photothermal cytotoxicity of Mito-BWQ in vitro, to further determine the subcellular distribution of Mito-BWQ, nuclei were imaged with Hoechst33342 (Hoechst), and Mito-BWQ-treated MCF-7 cells (Fig. 6c) and U87 cells (Fig. 6d) were stained with various commercially available organelle-selective tracers to identify the site of action of Mito-BWQ. As can be seen from the assays in the figure, the fluorescence images of Mito-BWQ overlap well with those of Mito-Tracker, a commercially available mitochondrial tracking dye. However, in the case of ER-Tracker, Lyso-Tracker, and Golgi-Tracker, the overlap is poor. These results provide support for the idea that Mito-BWQ localizes to the mitochondria, which may be the result of cation-attached triarylphosphine groups that help direct the dye to the mitochondria.

3.5. Photothermal conversion efficiency of Mito-BWQ inside MCF-7 cells

To study the photothermal conversion of Mito-BWQ in cells, temperature changes in Mito-BWQ-loaded MCF-7 cells were monitored using an infrared thermal camera (Fig. 7a) under NIR irradiation at 600 nm 1.5 W/cm². The local temperature of the irradiation site enhanced with increasing Mito-BWQ concentration (Fig. 7b-c). In particular, when the loaded Mito-BWQ concentration reached 50 µg/ml, it caused a rapid increase in the temperature of MCF-7 cells by 21 °C within 5 min, whereas in the absence of Mito-BWQ, this change was negligible. These

results indicate that Mito-BWQ can promote cell temperature under NIR irradiation. Next, we tested whether Mito-BWQ-based hyperthermia is sufficient to induce cell death.

3.6. Photothermal cytotoxicity (CCK-8 and Calcein AM/ PI staining Assay) of Mito-BWQ in Cells.

The photothermal therapy effect of Mito-BWQ was evaluated in vitro based on high PCE, solution stability and low toxicity. MCF-7 and U87 cells incubated with Mito-BWQ were irradiated with an 600 nm NIR laser for 5 min and cells incubated in the absence of Mito-BWQ loading were adopted as a negative control. As shown in Fig. 8a-b, there was a remarkable loss of viability of MCF-7 or U87 cells that were incubated with Mito-BWQ and treated with laser, while no significant difference was observed in the other groups. Moreover, as the Mito-BWQ loading concentration increased, the viability of their cells decreased obviously, and more than 80% of MCF-7 and U87 cells were killed after 5 min of irradiation. These results indicate that Mito-BWQ is an effective OSPA in vitro.

In addition, to further validate the PTT performance of Mito-BWQ in vitro, MCF-7 cells were stained with CalceinAM and PI solutions that can identify live and dead cells by emitting green or red fluorescence, respectively, and Mito-BWQ-loaded MCF-7 cells were alive (Fig. 8c) under no laser irradiation (green), confirming the low toxicity of Mito-BWQ, while the presence of external laser induced most cell death (red), and with increasing concentrations of Mito-BWQ loading, the red area became increasingly larger (Fig. 8d), again demonstrating that Mito-BWQ can be employed as an effective OSPA in vitro.

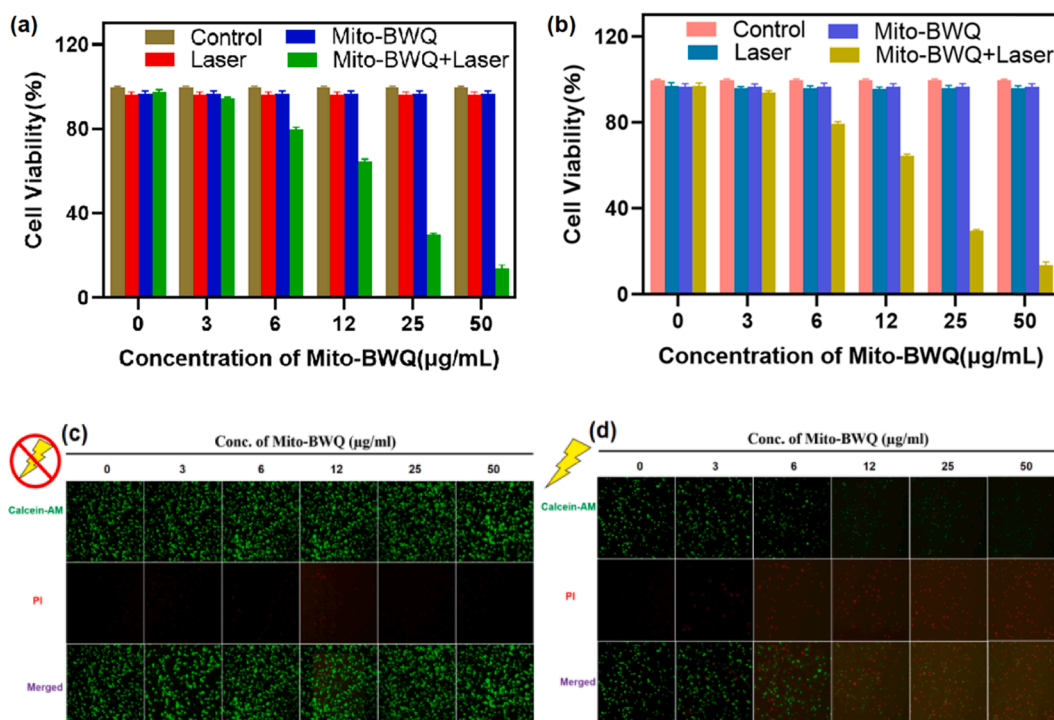


Fig. 8. Cell viability of MCF-7 cells (a) and U87 cells (b) treated with PBS, Laser, Mito-BWQ (Laser-) or Mito-BWQ (Laser +) at different concentrations. The cells were treated with PBS, Laser, Mito-BWQ (Laser-) or Mito-BWQ (Laser +) and incubated for 4 h at 37°C. Then CCK-8 assay was performed and absorbance in the CCK-8 assay was measured at 540 nm. (c) no laser and (d) laser cytotoxicity observed for MCF-7 cells incubated with Mito-BWQ. Confocal fluorescence images of MCF-7 cells obtained after incubation with Mito-BWQ as a function of concentration for 4 h. Dead/Live cells are detected as green or red by staining with Calcein-AM and PI, respectively. (For interpretation of the references to colour in this figure legend, the reader is referred to the web version of this article.)

3.7. *In vivo* xenografted tumor imaging and therapy by using Mito-BWQ.

Based on the *in vitro* efficient PTT cytotoxicity of Mito-BWQ, the *in vivo* antitumor efficacy of Mito-BWQ was subsequently investigated in MCF-7 rhabdomyolysis mice. To record the temperature changes (ΔT) at the tumor site under NIR irradiation, photothermal imaging was performed on the rhodoma mice. As shown in Fig. 9a, the temperature of the tumor sites in the laser and Mito-BWQ + Laser groups were detected by imaging in each minute during NIR irradiation. In laser group, the temperature of the tumor site increased extremely slowly and was about 36 °C after 5 min of 1.5 W/cm² NIR irradiation, which was accepted and tolerated by the lesions. However, under the same NIR laser irradiation, the temperature increased rapidly to about 49.5 °C in Mito-BWQ + Laser group. The imaging of the tumor localized area is shown in Fig. 9b. Fig. 9c presents the ΔT of the tumor site during NIR irradiation. The ΔT of the laser group was about 12 °C, while the value of the Mito-BWQ + Laser group was about 24.5 °C, which was two times higher than that of the laser group. And it is believed that the temperature of cancer cells above 45 °C leads to irreversible tissue damage and necrosis of the lesions [38], so that tumors can be extinguished in the Mito-BWQ + Laser group.

The biodistribution of Mito-BWQ in mice was further detected by fluorescence imaging. Mito-BWQ was applied to the tumors of nude mice with breast cancer xenograft tumors, and the kinetics of Mito-BWQ were measured at 0.5, 2, 4, 12, 24, 48, and 72 h (Fig. 9d). Biofluorescence reached its highest at 12 h after Mito-BWQ treatment, which we attribute to the fact that Mito-BWQ was most fully bound to the mitochondria in the tumor tissue at this time. Moreover, Mito-BWQ fluorescence was still detected at 72 h. This finding indicates that Mito-BWQ accumulates mainly in tumors and is retained for a long time without rapidly spreading to other organs. This favorable accumulation behavior may reduce repeated drug injections and promote PTT *in vivo*. In addition, to detect whether Mito-BWQ could be distributed in organs

other than tumors, *in vitro* fluorescence images of normal organs and tumors were obtained after 24, 48, and 72 h (Fig. 9e-f). Stronger fluorescence was observed in the liver and kidney, revealing diffusion and preferential accumulation of Mito-BWQ. Little or no fluorescence was found in other healthy tissues. Although Mito-BWQ was conserved in healthy organs, this OSPA was not overtly toxic, as revealed by subsequent examination.

To verify the anti-tumor effects of Mito-BWQ *in vivo*, rhabdomyolysis mice were treated with PBS(Laser-), Laser+, PBS(Laser +), Mito-BWQ(Laser-), and Mito-BWQ(Laser +). The MCF-7 tumor-bearing mice were irradiated for 5 min with a 600 nm laser (1.5 W/cm²) after 12 h to perform effective PTT (Fig. 10a). As shown in Fig. 10c and 10d, in the experimental groups including PBS(Laser-), Laser+, PBS(Laser +) and Mito-BWQ(Laser-) group, the tumors grew rapidly and had no obvious inhibitory effect, which also showed that Mito-BWQ had low biological toxicity. In contrast, the Mito-BWQ(Laser +) group presented good tumor suppression and no significant change in body weight (Fig. 10e), highlighting the strong tumor inhibition potential of Mito-BWQ. To determine the biosafety of Mito-BWQ, after treatment, mice were executed and tumors were removed (Fig. 10f), and H&E-stained sections of their major organs, including heart, liver, spleen, lungs, and kidneys, were evaluated (Fig. 10g). The results showed no significant necrosis or damage to the major organs in the five groups, indicating that Mito-BWQ has no significant toxic effects on living organisms. All these results reveal that OSPA is an effective novel PTT drug for anti-tumor application.

4. Conclusion

In conclusion, we have developed a novel mitochondria-targeted OSPA for enhanced PTT. The new OSPA reported here, Mito-BWQ, contains two major components, the thiazole orange maternal unit for NIR absorption and triphenylphosphonium mitochondrial localizing unit. The

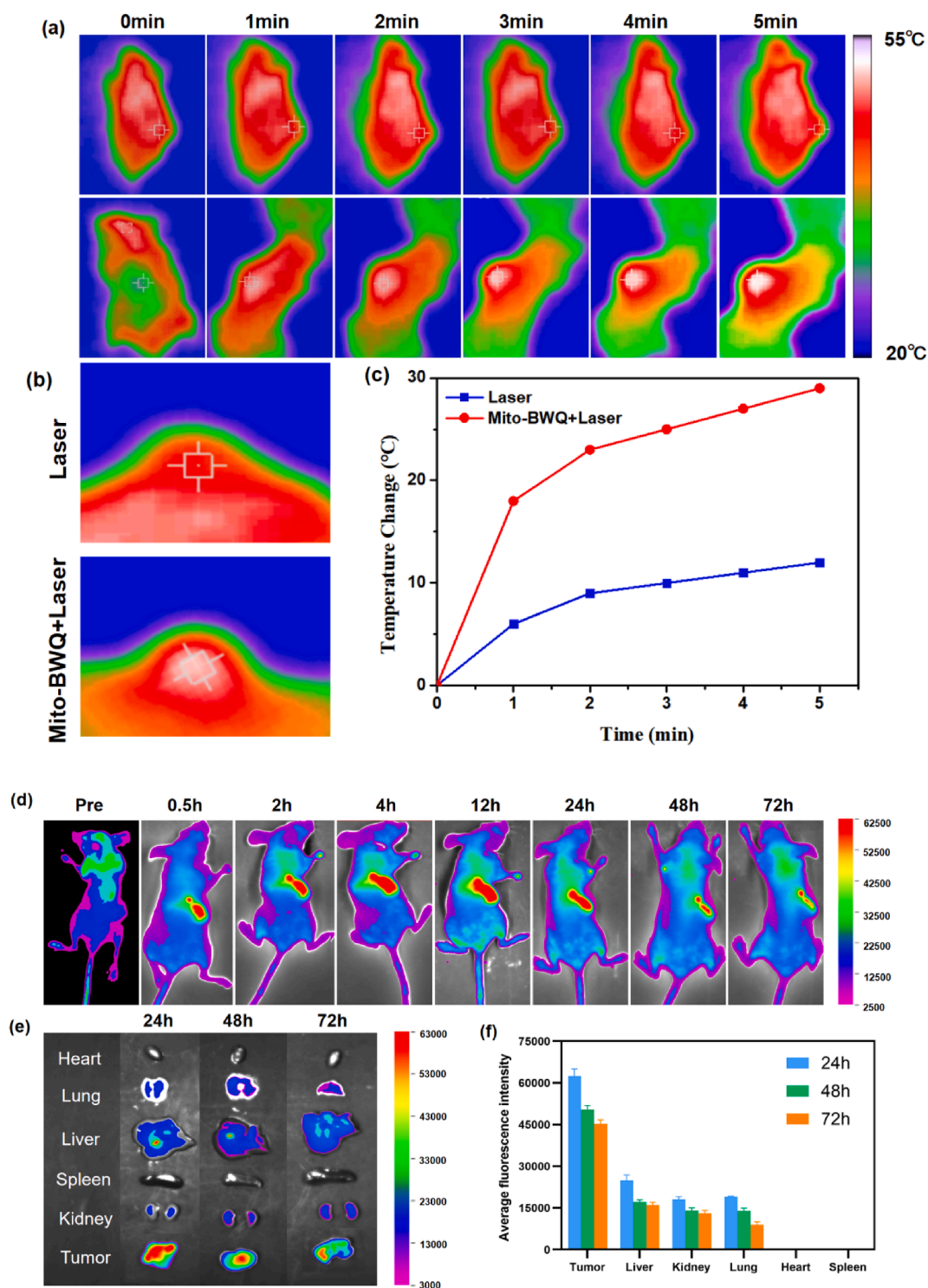


Fig. 9. In vivo xenografted photothermal imaging and fluorescence imaging. (a) Photothermal images of tumor site in Laser group (injected with normal saline) and Mito-BWQ + Laser group (injected with Mito-BWQ) during 5 min irradiation of 1.5 W/cm² NIR. (b) Local tumor area temperature images of the mice at the fifth min of NIR irradiation. (c) Temperature change (ΔT) of tumor sites during NIR irradiation. (d) Fluorescence images of mice bearing MCF-7 tumors treated with Mito-BWQ three days after injection. (e) Fluorescence images and (f) comparison of the fluorescence intensity from tumors and main tissues 24, 48, and 72 h post injection ($n = 3$).

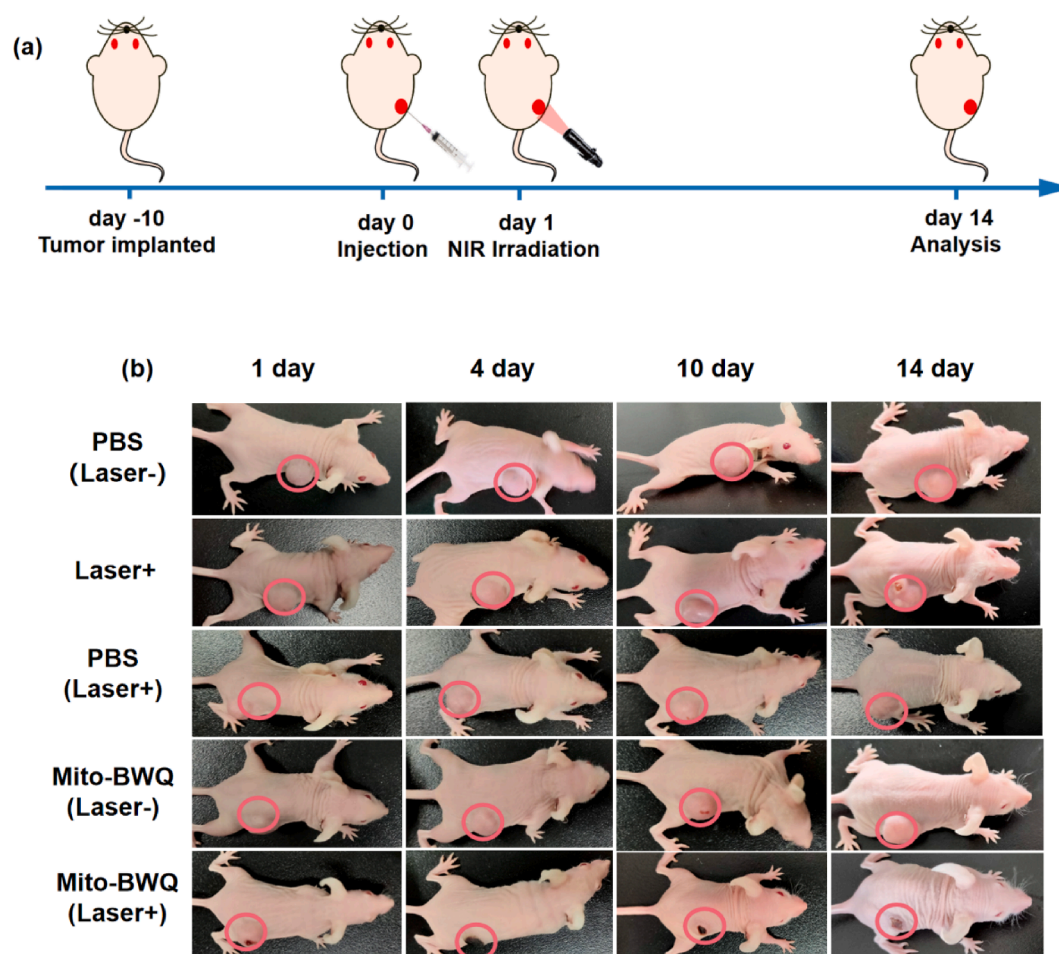


Fig. 10. MCF-7 tumor-bearing mice photothermal therapy. (a) Schematic depiction of the treatment of breast cancer mouse model with Mito-BWQ. (b) Pictures of different groups of mice at day 1, day 4, day 10 and day 14 after photothermal treatment. (c) Weights of the tumors after in different groups therapies (mean \pm SD, $n = 5$, $***P < 0.001$) at the end of the antitumor study. (d) The relative tumor volume (tumor volume divided by initial volume) in various mice groups (mean \pm SD, $n = 5$, $***P < 0.001$) and (e) Changes in weight of mice in different groups over time (mean \pm SD, $n = 5$, $*P < 0.05$). (f) Images of the tumors and (g) histological images of major organs after photothermal therapy.

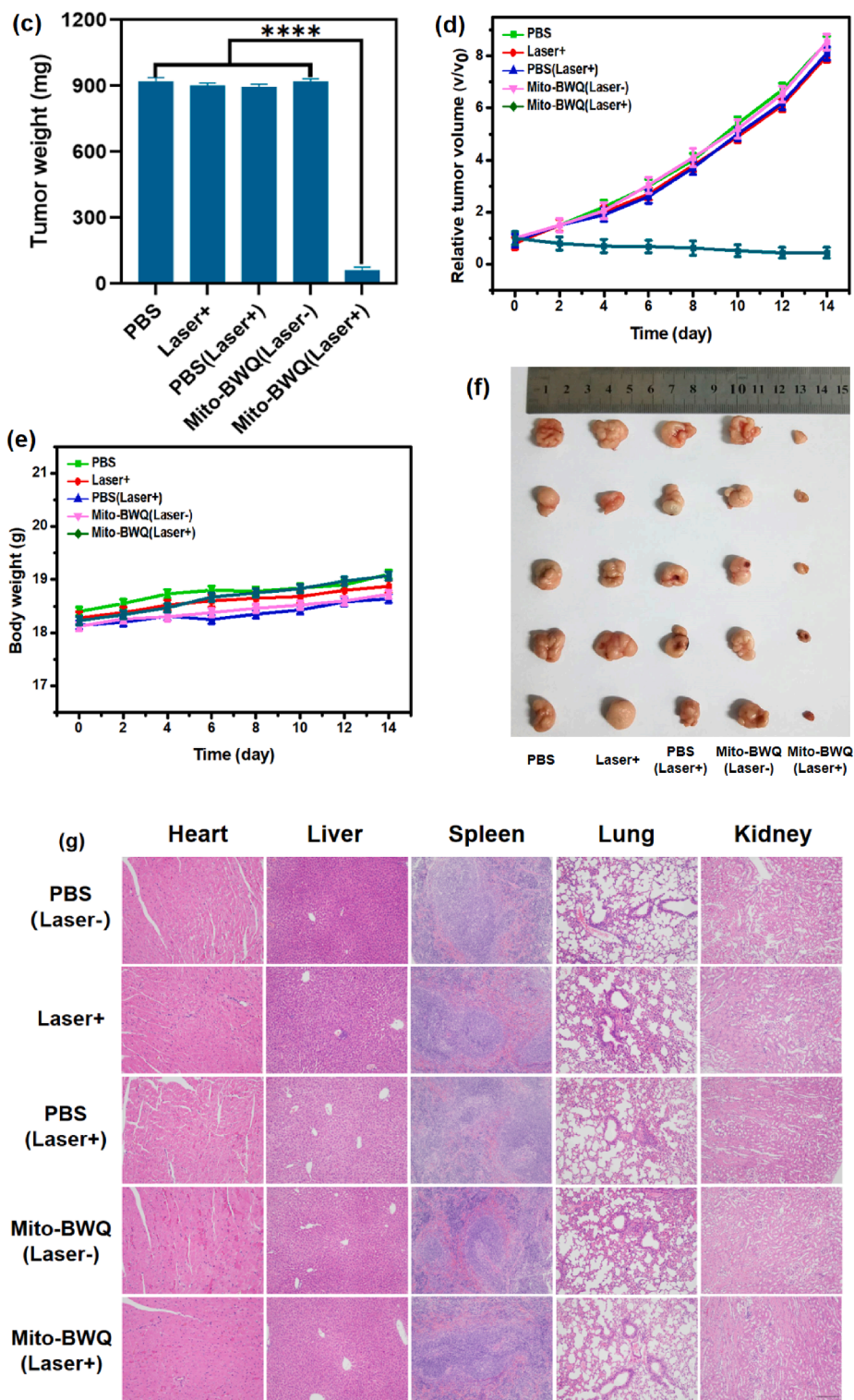


Fig. 10. (continued).

synthesized Mito-BWQ presents high photothermal conversion efficiency (PCE), low cytotoxicity and good biosafety in PTT. In vivo tests show that an excellent tumor suppressive effect can be achieved with the Mito-BWQ. We believe this work provides a vital starting point for the construction of thiazole orange-based PTT agents that could contribute to drive in-depth progress in PA-based anti-cancer research and therapeutics. And further applications of Mito-BWQ to bind targeting ligands and thus specifically navigate to tumor tissues are underway in our laboratory.

Declaration of Competing Interest

The authors declare that they have no known competing financial interests or personal relationships that could have appeared to influence the work reported in this paper.

Acknowledgement

Zhen-xing Pan: Methodology, Investigation, Formal analysis. **Ya-kun Wang:** Software, Data curation. **Wei Long:** Methodology, Visualization. **Ze-feng Chen:** Software, Data curation. **Ni-ping Chen:** Resources, Visualization. **Yao-xun Zeng:** Resources, Visualization. **Jiong-peng Yuan:** Resources, Visualization. **Xujie Liu:** Project administration, Supervision, Conceptualization, Writing - review & editing. **Yujing Lu:** Project administration, Supervision, Conceptualization, Writing - review & editing. **Yan He:** Project administration, Supervision, Conceptualization, Writing - review & editing, Funding acquisition. **Kun Zhang:** Project administration, Supervision, Conceptualization, Writing - review & editing.

5. Funding sources

This work was supported by the National Natural Science Foundation of China (grant numbers No.81803000)

Disclosure.

The authors declare no competing financial interest.

Appendix A. Supplementary data

Supplementary data to this article can be found online at <https://doi.org/10.1016/j.bioorg.2021.104954>.

References

- [1] A. Husby, J. Wohlfahrt, N. Oyen, M. Melbye, Pregnancy duration and breast cancer risk, *Nat Commun* 9 (1) (2018) 4255.
- [2] P. Chuntova, K.M. Downey, B. Hegde, N.D. Almeida, H. Okada, Genetically Engineered T-Cells for Malignant Glioma: Overcoming the Barriers to Effective Immunotherapy, *Front Immunol* (2018).
- [3] J. Xu, P. Yang, M. Sun, H. Bi, B. Liu, D. Yang, S. Gai, F. He, J. Lin, Highly Emissive Dye-Sensitized Upconversion Nanostructure for Dual-Photosensitizer Photodynamic Therapy and Bioimaging, *ACS Nano* 11 (4) (2017) 4133–4144.
- [4] M.R. Rutkowski, T.L. Stephen, J.R. Conejo-Garcia, Anti-tumor immunity: Myeloid leukocytes control the immune landscape, *Cellular Immunology* 278 (1–2) (2012) 21–26.
- [5] B.A. Chabner, T.G.R. Jr, Chemotherapy and the war on cancer, *Nat Rev Cancer* 5 (1) (2017) 65–72.
- [6] D. Jaque, L. Martinez Maestro, B. del Rosal, P. Haro-Gonzalez, A. Benayas, J. L. Plaza, E. Martin Rodriguez, J. Garcia Sole, Nanoparticles for photothermal therapies, *Nanoscale* 6 (16) (2014) 9494–9530.
- [7] A.M. Brouwer, Standards for photoluminescence quantum yield measurements in solution (IUPAC Technical Report), *Pure Appl. Chem.* 83 (2011) 2213–2228.
- [8] M. Zhou, R. Zhang, M. Huang, W. Lu, S. Song, M. Melancon, M. Tian, D. Liang, C. Li, A Chelator-Free Multifunctional [Cu-64]CuS Nanoparticle Platform for Simultaneous Micro-PET/CT Imaging and Photothermal Ablation Therapy, *Journal of the American Chemical Society* 132 (2010) 15351–15358.
- [9] N.K. Prasad, K. Rathinasamy, D. Panda, D. Bahadur, Mechanism of cell death induced by magnetic hyperthermia with nanoparticles of γ -Mn_xFe_{2-x}O₃ synthesized by a single step process, *Journal of Materials Chemistry* 17 (48) (2007).
- [10] B. Nikoobakht, M.A. El-Sayed, Preparation and Growth Mechanism of Gold Nanorods (NRs) Using Seed-Mediated Growth Method, *Chemistry of Materials* 15 (10) (2003) 1957–1962.
- [11] Y. Xia, W. Li, C.M. Cobley, J. Chen, X. Xia, Q. Zhang, M. Yang, E.C. Cho, P. K. Brown, Gold Nanocages: From Synthesis to Theranostic Applications, *Accounts of Chemical Research* 44 (10) (2011) 914–924.
- [12] K. Yang, L. Feng, X. Shi, Z. Liu, Nano-graphene in biomedicine: theranostic applications, *Chem. Soc. Rev.* 42 (2) (2013) 530–547.
- [13] X. Huang, S. Tang, X. Mu, Y. Dai, G. Chen, Z. Zhou, F. Ruan, Z. Yang, N. Zheng, Freestanding palladium nanosheets with plasmonic and catalytic properties, *Nature Nanotechnology* 6 (1) (2011) 28–32.
- [14] M. Zhou, R. Zhang, M. Huang, W. Lu, S. Song, M.P. Melancon, M. Tian, D. Liang, C. Li, A Chelator-Free Multifunctional [64Cu]CuS Nanoparticle Platform for Simultaneous Micro-PET/CT Imaging and Photothermal Ablation Therapy, *Journal of the American Chemical Society* 132 (43) (2010) 15351–15358.
- [15] J. Li, F. Jiang, B. Yang, X.-R. Song, Y. Liu, H.-H. Yang, D.-R. Cao, W.-R. Shi, G.-N. Chen, Topological insulator bismuth selenide as a theranostic platform for simultaneous cancer imaging and therapy, *Scientific Reports* 3 (1) (2013) 1998.
- [16] S.S. Chou, B. Kaehr, J. Kim, B.M. Foley, M. De, P.E. Hopkins, J. Huang, C. J. Brinker, V.P. Dravid, Chemically exfoliated MoS₂ as near-infrared photothermal agents, *Angew Chem Int Ed Engl* 52 (15) (2013) 4160–4164.
- [17] Z. Liu, A.C. Fan, K. Rakhra, S. Sherlock, A. Goodwin, X. Chen, Q. Yang, D. W. Felsler, H. Dai, Supramolecular stacking of doxorubicin on carbon nanotubes for in vivo cancer therapy, *Angew Chem Int Ed Engl* (2009).
- [18] A.A. Bhirde, V. Patel, J. Gavard, G. Zhang, A.A. Sousa, A. Masedunskas, R. D. Leapman, R. Weigert, J.S. Gutkind, J.F. Rusling, Targeted killing of cancer cells in vivo and in vitro with EGF-directed carbon nanotube-based drug delivery, *ACS Nano* (2009).
- [19] C.A. Poland, R. Duffin, I. Kinloch, A. Maynard, W.A.H. Wallace, A. Seaton, V. Stone, S. Brown, W. MacNee, K. Donaldson, Carbon nanotubes introduced into the abdominal cavity of mice show asbestos-like pathogenicity in a pilot study, *Nature Nanotechnology* 3 (7) (2008) 423–428.
- [20] A.A. Bhirde, V. Patel, J. Gavard, G. Zhang, A.A. Sousa, A. Masedunskas, R. D. Leapman, R. Weigert, J.S. Gutkind, J.F. Rusling, Targeted Killing of Cancer Cells in Vivo and in Vitro with EGF-Directed Carbon Nanotube-Based Drug Delivery, *ACS Nano* 3 (2) (2009) 307–316.
- [21] A. Yuan, J. Wu, X. Tang, L. Zhao, F. Xu, Y. Hu, Application of near-infrared dyes for tumor imaging, photothermal, and photodynamic therapies, *J Pharm Sci* (2013).
- [22] N. Muhanna, C.S. Jin, E. Huynh, H. Chan, Y. Qiu, W. Jiang, L. Cui, L. Burgess, M. K. Akens, J. Chen, J.C. Irish, G. Zheng, Phototheranostic Porphyrin Nanoparticles Enable Visualization and Targeted Treatment of Head and Neck Cancer in Clinically Relevant Models, *Theranostics* (2015).
- [23] H.S. Jung, P. Verwilt, A. Sharma, J. Shin, J.L. Sessler, J.S. Kim, Organic molecule-based photothermal agents: an expanding photothermal therapy universe, *Chem Soc Rev* (2018).
- [24] M.M. Wright, A.G. Howe, V. Zaremborg, Cell membranes and apoptosis: role of cardiolipin, phosphatidylcholine, and anticancer lipid analogues, *Biochem Cell Biol* (2004).
- [25] F. Zhou, S. Wu, B. Wu, W.R. Chen, D. Xing, Mitochondria-targeting single-walled carbon nanotubes for cancer photothermal therapy, *Small* 7 (19) (2011) 2727–2735.
- [26] Z. Wang, F. Cai, X. Chen, M. Luo, L. Hu, Y. Lu, The role of mitochondria-derived reactive oxygen species in hyperthermia-induced platelet apoptosis, *PLoS One* (2013).
- [27] S. Chen, Q. Lei, W.-X. Qiu, L.-H. Liu, D.-W. Zheng, J.-X. Fan, L. Rong, Y.-X. Sun, X.-Z. Zhang, Mitochondria-targeting, “Nanoheater” for enhanced photothermal/chemo-therapy, *Biomaterials* 117 (2017) 92–104.
- [28] B.P. Shah, N. Pasquale, G. De, T. Tan, J. Ma, K.-B. Lee, Core-Shell Nanoparticle-Based Peptide Therapeutics and Combined Hyperthermia for Enhanced Cancer Cell Apoptosis, *ACS Nano* 8 (9) (2014) 9379–9387.
- [29] M.P. Murphy, R.A.J. Smith, Targeting Antioxidants to Mitochondria by Conjugation to Lipophilic Cations, *Annual Review of Pharmacology and Toxicology* 47 (1) (2007) 629–656.
- [30] P. Wipf, J. Xiao, Convergent Approach to (E)-Alkene and Cyclopropane Peptide Isosteres, *Organic Letters* 7 (1) (2005) 103–106.
- [31] K.L. Horton, K.M. Stewart, S.B. Fonseca, Q. Guo, S.O. Kelley, Mitochondria-Penetrating Peptides, *Chemistry & Biology* 15 (4) (2008) 375–382.
- [32] L.F. Yousif, K.M. Stewart, S.O. Kelley, Targeting Mitochondria with Organelle-Specific Compounds: Strategies and Applications, *ChemBioChem* 10 (12) (2009) 1939–1950.
- [33] H.S. Jung, J. Han, J.-H. Lee, J.H. Lee, J.-M. Choi, H.-S. Kweon, J.H. Han, J.-H. Kim, K.M. Byun, J.H. Jung, C. Kang, J.S. Kim, Enhanced NIR Radiation-Triggered Hyperthermia by Mitochondrial Targeting, *Journal of the American Chemical Society* 137 (8) (2015) 3017–3023.
- [34] W. Sun, S. Guo, C. Hu, J. Fan, X. Peng, Recent Development of Chemosensors Based on Cyanine Platforms, *Chemical Reviews* 116 (14) (2016) 7768–7817.
- [35] J. Zhang, Z. Liu, P. Lian, J. Qian, X. Li, L. Wang, W. Fu, L. Chen, Wei X.; Li C. via Selective imaging and cancer cell death pH switchable near-infrared fluorescence and photothermal effects, *Chem Sci* (2016).
- [36] Q. Tian, F. Jiang, R. Zou, Q. Liu, Z. Chen, M. Zhu, S. Yang, J. Wang, J. Wang, J. Hu, Hydrophilic Cu₉S₅ Nanocrystals: A Photothermal Agent with a 25.7% Heat Conversion Efficiency for Photothermal Ablation of Cancer Cells in Vivo, *ACS Nano* 5 (12) (2011) 9761–9771.
- [37] G.Y. Pan, H.R. Jia, Y.X. Zhu, et al., A Dual Channel Activatable Cyanine Dye for Mitochondrial Imaging and Mitochondria-Targeted Cancer Theranostics[J], *Acs Biomaterials Science & Engineering* (2017) acsbiomaterials.7b00480.
- [38] G. Gao, Y.W. Jiang, Y. Guo, H.R. Jia, X. Cheng, Y. Deng, X.W. Yu, Y.X. Zhu, H. Y. Guo, W. Sun, X. Liu, J. Zhao, S. Yang, Z.W. Yu, F.M.S. Raya, G. Liang, F.G. Wu, Enzyme-Mediated Tumor Starvation and Phototherapy Enhance Mild-Temperature Photothermal Therapy, *Advanced Functional Materials* 30 (16) (2020).